Microstructure and Mechanical Properties of Friction Stir Welded Aluminum 5083 Alloy Joints

Jawdat Al-Jarrah
Fire and Safety Engineering Department, Prince Al-Hussein Bin Abdullah II Academy for Civil Protection, Al-Balqa Applied University, Jordan
jawdatj@yahoo.com (corresponding author)

Mohamed H. Frihat
Mechanical Engineering Department, Al-Huson University College, Al-Balqa Applied University, Jordan
m.frihat@bau.edu.jo

Maen Al-Rashdan
Mechanical Engineering Department, Al-Huson University College, Al-Balqa Applied University, Jordan
mmrashdan@bau.edu.jo

Firas Al Quran
Mechanical Engineering Department, Al-Huson University College, Al-Balqa Applied University, Jordan
firas.q@bau.edu.jo

Deya A. Al Qasy
Ministry of Education, Jordan
deya2941982@yahoo.com

Received: 2 September 2025 | Revised: 13 December 2025 and 18 March 2026 | Accepted: 19 March 2026

 DOI: https://doi.org/10.48084/etasr.14474

ABSTRACT

This research involved joining two 6-mm-thick 5083 aluminum alloy plates using Friction Stir Welding (FSW) and analyzing the mechanical properties of the resulting joints. Different joints were produced by varying the rotation speed from 400 rpm to 1,600 rpm in 200-rpm increments. Seven levels of welding speed were also utilized, ranging from 20 mm/min to 140 mm/min. The grain size and microhardness of the stir zone are influenced by the heat generated during welding. The grain size increased from 4.3 µm to 7.3 µm when the welding speed was 20 mm/min, while the microhardness decreased from 46 HV to 40 HV as the rotational speed increased from 400 rpm to 1600 rpm. A strong welded joint with an ultimate tensile strength of 210 MPa was produced at a rotational speed of 1200 rpm and a welding speed of 80 mm/min. The Rotation-per-Feed (RPF) ratio affects the mechanical properties of welded joints. RPF values between 12 and 18 were found to produce sound weldments with ultimate tensile strengths greater than 190 MPa. Additionally, it was observed that keeping the welding speed constant increases the ultimate tensile strength with rotational speed until it reaches an optimum value. Further increases in rotational speed led to a drop in the strength of the welded joint.

Keywords-friction stir welding; aluminum alloy; ultimate tensile strength; welding

I. INTRODUCTION

The aluminum 5083 alloy is widely used in the shipbuilding and automotive sectors, where corrosion resistance and a good strength-to-weight ratio are required [1-3]. However, reliable joints are necessary for connecting aluminum parts in various applications. Some joints, such as rivets, are expensive, while others, such as welds, are more durable and cheaper [4, 5]. Welding aluminum alloys can result in tiny voids or bubbles in the joint, due to the tendency of hydrogen to dissolve in molten aluminum [6]. Aluminum alloys can be welded using either fusion or solid-state welding techniques [7]. Fusion welding involves chemically bonding aluminum in the molten state.

Proper filler materials and a shield of inert gas in the weld zone are often required to prevent oxidation of the aluminum alloy, as well as surface preparation [8]. Fusion welding includes Metal Inert Gas (MIG), Tungsten Inert Gas (TIG), arc welding, and laser welding. However, fusion welding's high heat input reduces the strength of the resulting aluminum alloy joints [9]. In contrast, solid-state welding produces joints in a semisolid state where the temperature of the welding zone is lower than the melting point of the base metal. Additionally, no filler or inert gas shield is necessary. Nevertheless, many welding methods, such as ultrasonic, explosion, friction, cold, and roll welding, are used to weld metal in a solid state [10-13]. Friction Stir Welding (FSW) is a solid-state joining process, which is widely used, initially for aluminum alloys [14-16]. The FSW method is becoming more popular due to its economic advantages over conventional methods, with the joints being highly efficient and exhibiting a smaller heat-affected zone [17]. Other benefits of the FSW process include using a non-consumable tool and being able to weld thick plates in a single pass, which results in significant time and cost savings for welded joints [18]. The FSW welding tool consists of a shoulder and an extended non-consumable pin. FSW occurs when the rotating tool is forced down into the weld line under sufficient pressure, generating frictional heat, raising the material temperature, and causing it to plastically deform radially. The pin mixes the plastic material in the stir zone [11]. The two main FSW parameters are rotational speed and welding speed, which control the heat generated during the welding process [19]. Other welding parameters include the axial force applied to the workpiece by the welding tool shoulder, the tilt angle of the welding tool, and the tool geometry [20]. Joint efficiency was measured by comparing the strength of joints produced by FSW to that of the base metal [21]. However, joints produced by FSW are always weaker than the base metal under different combinations of welding parameters [22]. Additionally, welding parameters contribute to welding defects and the microstructure of the weld zone [23]. The rate of heat generated during the welding process is due to the relative motion between the welding tool and the workpiece [24]. As the welding tool's rotational speed increases, so does the rate of heat generation [25]. However, welding speed controls heat dissipation from the workpiece, particularly when using natural air cooling. As the welding speed increases, the area exposed to air increases, which is directly proportional to the rate of heat release [26]. At a rotational speed of 1000 rpm and a welding speed of 30 mm/min, sufficient heat is generated and transferred to the tool shoulder face. This results in the melting of the aluminum alloy layer in contact with the shoulder and its uneven smearing beneath the shoulder face. However, at a higher welding speed of 90 mm/min, no aluminum alloy melting occurred, and the weld joint surface was smoother under the tool shoulder [27]. To produce defect-free joints in FSW, it is essential to balance the heat generated and dissipated during welding. Both generated and dissipated heat affect grain size, Vickers microhardness, mechanical properties, and weld defects. Thus, the correlation between these two welding parameters, such as Rotational per Feed (RPF) or Feed per Rotation (FPR), provides insights into the relationship between weldment quality and these parameters [28]. The RPF is more related to the generated heat, while the FPR is more related to the dissipated heat. This study aims to evaluate the effects of welding and rotational speeds on the mechanical and microstructural behavior of 5083 aluminum alloy welded plates. Additionally, the goal is to correlate the properties of the welded joints with the RPF. The welding parameters were chosen to cover a wide range of RPF, from 2.86 r/mm to 80 r/mm. The grain size, microhardness, and strength of the welded joints were measured and analyzed with respect to the RPF factor.

II. EXPERIMENTAL METHOD

The chemical composition of the 5083-aluminum alloy is shown in Table I. The mechanical properties of the alloy as a base material were measured as: yield stress (160 MPa), ultimate tensile strength (306 MPa), and Vickers microhardness (56 HV).

TABLE I. CHEMICAL COMPOSITION OF AL ALLOY

Comp.	Mg	Mn	Cu	Si	Fe	Ni	Zn	Ti	Cr	Al
Wt%	5.56	0.53	0.032	<0.01	0.29	<0.01	0.024	0.014	0.063	93.47

Rectangular plates measuring 300 mm x 150 mm were cut from a 6-mm-thick aluminum 5083 alloy sheet to create butt-welded joints. FSW was performed using a vertical milling machine. To ensure precise joint formation during FSW, the aluminum plates were securely held by a custom-designed fixture specifically adapted for the milling machine. The welding tool was made of high-carbon AISI 1065 steel and featured a 20-mm flat shoulder and a 6-mm square pin measuring 5.8 mm in height. The FSW parameters spanned a wide range of welding and tool rotational speeds. Two sets of welding parameters were chosen. The first set was processed at seven welding speeds (20 mm/min, 40 mm/min, 60 mm/min, 80 mm/min, 100 mm/min, 120 mm/min, and 140 mm/min) and three rotational speeds (400 rpm, 1000 rpm, and 1600 rpm). The second set included seven rotational speeds (400 rpm, 600 rpm, 800 rpm, 1000 rpm, 1200 rpm, 1400 rpm, and 1600 rpm) and three welding speeds (20 mm/min, 80 mm/min, and 140 mm/min). The force applied by the tool shoulder against the upper face of the workpiece was kept constant at 8 kN using a spring-loaded unit attached to the welding tool. A single pass was performed for each joint. Three joints were produced at each combination of welding speed and rotational speed. The joints were then subjected to tensile and microhardness tests. The tensile test specimens were cut transversely, perpendicular to the welding line. The specimens had a gauge diameter of 12 mm and a gauge length of 90 mm, as shown in Figure 1, and adhered to ASTM E8M. The average of three readings was calculated and recorded.

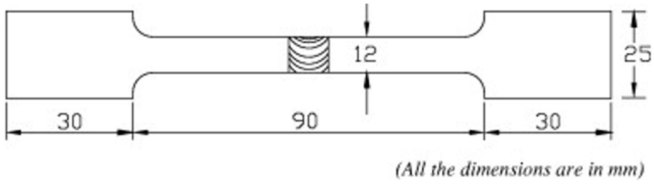

Fig. 1. Dimensions of tensile specimen.

According to ASTM E384, a Vickers microhardness tester was used to measure microhardness at a load of 0.5 kgf and a dwell time of 10 s. Measurements were taken in a stir-welding zone with 1 mm spacing between Vickers indentations. Five indentations were measured and recorded for each stir zone. This study presents the average of the five microhardness readings. Microstructure samples were cut from the stir-welding zone and examined under an optical microscope at 90x magnification. To reveal the grain structure, the microstructure samples were etched using Keller's reagents, as specified in ASTM E407. The grain size of the stir zone was measured using light microscopy images.

III. RESULTS AND DISCUSSION

A. Microstructure and Macrostructure Analysis

Optical microscopy was used to study the microstructure of aluminum 5083 alloy joints produced by FSW across all combinations of rotational and welding speeds. During the FSW process, heat softens the material inside the stir zone. The pin mixes this plasticized zone, becoming adaptable and allowing for grain refinement [29]. Figure 2 shows the center of the stir zone microstructure for samples joined at a welding speed of 20 mm/min and rotational speeds of 400 rpm and 1,600 rpm. The stir zone microstructure shows equiaxed grains at 400 rpm. The heat generated during FSW is due to friction between the welding tool and the welded plates [27], which increases with the relative speed between the mating surfaces [12]. In this study, the specimens were allowed to cool naturally. Therefore, the cooling time of the specimen depends on the amount of heat generated during FSW [19]. The stir zone softens further as the input heat increases, raising its temperature and providing sufficient time for grain growth [30]. Coarse grains were obtained at a higher rotational speed of 1600 rpm with a constant welding speed of 20 mm/min, as depicted in Figure 2 (b). However, increasing the welding speed reduces the heat generated per unit length when the rotational speed is kept constant. Figure 3 displays the fine-grained microstructure of the stir zone produced at a rotational speed of 1,600 rpm and a welding speed of 140 mm/min.

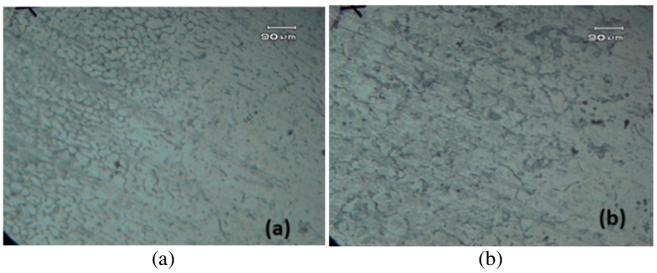

(a) (b)

Fig. 2. Microstructure of the welding zone produced at 20 mm/min with a rotational speed of: (a) 400 rpm and (b) 1600 rpm.

The heat generated during the FSW process is directly proportional to the tool's rotational speed per unit feed. Alternatively, it can be kept constant by maintaining a constant welding speed. The surface appearance of the weld joints is affected by the RPF rate, which controls the amount of heat generated and introduced to the welding zone. Figure 4 portrays the appearance of welded joints produced at a rotational speed of 1000 rpm and welding speeds of 20 mm/min, 80 mm/min, and 140 mm/min (i.e., RPF values of 50 r/mm, 12.5 r/mm, and 7.14 r/mm). A smooth, fine surface joint is produced at 50 r/mm, as shown in Figure 4 (a). Onion rings then appear at an RPF of 12.5 r/mm, as presented in Figure 4 (b). At a higher welding speed (RPF = 7.14), the onion rings become coarser, as illustrated in Figure 4 (c). Figure 5 demonstrates the surface appearance of the welded joints at a rotational speed of 1,600 rpm and welding speeds of 20 mm/min and 100 mm/min. The RPF values are 80 r/mm and 16 r/mm, respectively. At an RPF of 80 r/mm, extra heat is generated and introduced to the welding joints. This increases the temperature of the welded zone, causing the aluminum layer to become more fluid under the tool shoulder face. It smears easily and solidifies more on the advanced side than the retreating side when exposed briefly to ambient air, as depicted in Figure 5 (a).

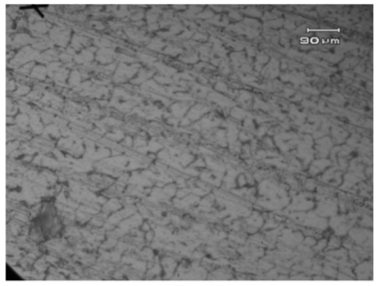

Fig. 3. Microstructure of the stir zone produced at 1600 rpm and 140 mm/min.

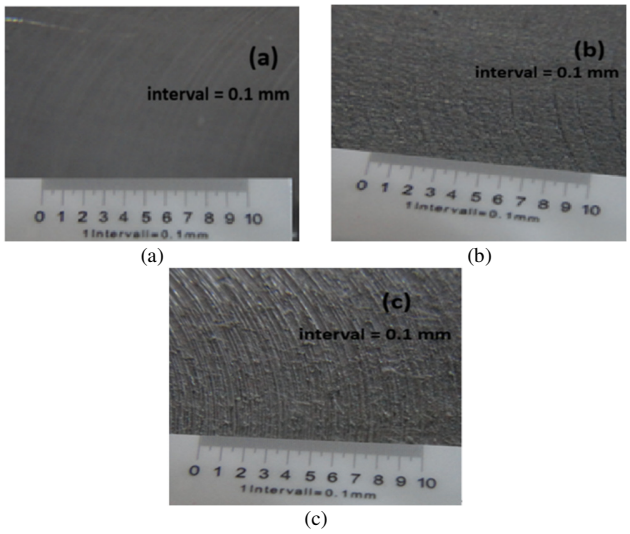

(a) (b)

(c)

Fig. 4. Appearance of the welded joint at 1000 rpm: (a) 20 mm/min, (b) 80 mm/min, and (c) 140 mm/min.

However, Figure 5 (b) exhibits that when the RPF is reduced to 16 r/min, less heat is introduced to the welding zone, resulting in a fine, smooth surface with clear onion rings. However, joints produced at a lower RPF (6.67 r/min) with a rotational speed of 800 rpm and a welding speed of 120 mm/min exhibit coarse onion rings and minor surface pitting,

as shown in Figure 6 (a). This may be attributed to two reasons: first, low heat is introduced into the welding zone, which reduces the fluidity of the aluminum layer under the shoulder surface, and second, there is a lack of stirring of the welding zone during the welding process. Larger pitting appears when the welding speed increases to 140 mm/min, and the rotational speed decreases to 400 rpm, as presented in Figure 6 (b). In this case, the RPF is 2.86, insufficient heat is generated, and little heat is introduced to the welding zone, resulting in a low temperature in the latter. Consequently, the aluminum layers beneath the tool shoulder require a high shear force to move due to their lack of fluidity, leading to aluminum material loss from the hard tool shoulder, leaving a large pit behind.

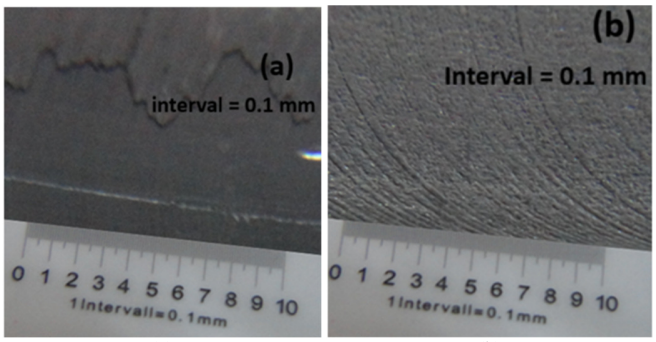

(a) (b)

Fig. 5. Appearance of the welded joints at 1600 rpm with: (a) 20 mm/min and (b) 100 mm/min.

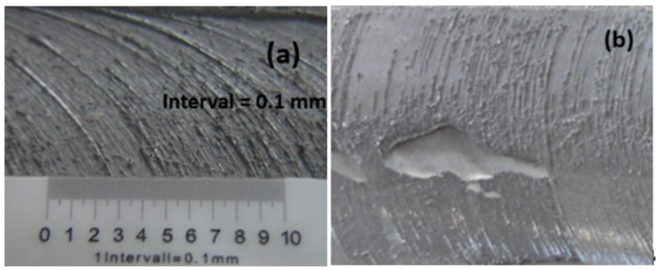

(a) (b)

Fig. 6. Appearance of welded joint produced by 140 mm/min with: (a) 800 rpm and (b) 400 rpm.

Figure 7 displays how grain size varies with RPF. That is, grain size increases as RPF increases, along with the heat generated during welding, but not linear/linearly. Grain size increases rapidly from 2.1 µm to 5.2 µm as RPF increases from 2.85 r/mm to 25 r/mm, from 2.1 µm to 5.2 µm, respectively. However, the grain size increases more slowly when the RPF exceeds 26 r/mm. Increasing the welding speed, however, reduces the heat generation rate at the stir zone during FSW. The grain size in the center of the stir zone decreases from 6.2 µm at a welding speed of 20 mm/min to 3.8 µm at a welding speed of 100 mm/min, with a constant rotational speed of 1200 rpm, as illustrated in Figure 8. Figure 9 displays the effect of rotational speed on grain size. As the rotational speed increases, so does the heat introduced to the welding zone, giving the grain sufficient time to grow while cooling. As the rotational speed increases from 400 rpm to 1600 rpm, it is observed that the grain size increases from 4.8 µm to 7.3 µm, while the welding speed is kept constant at 20 mm/min.

B. Mechanical Properties

During FSW, the material in the stir zone softens due to frictional heating and is mixed by the pin. Thus, there are many mechanisms that modify the strength of the stir zone. The primary mechanism is solution strengthening, in which magnesium (Mg) is the primary alloying element in aluminum 5083 alloys. Mg remains in solid solution during FSW, resulting in strengthening through solution-dislocation interactions. Other elements, such as manganese, copper, iron, and silicon, precipitate at grain boundaries via precipitation hardening [31]. This study investigated and analyzed the strength of welded joints under different combinations of welding and rotational speeds.

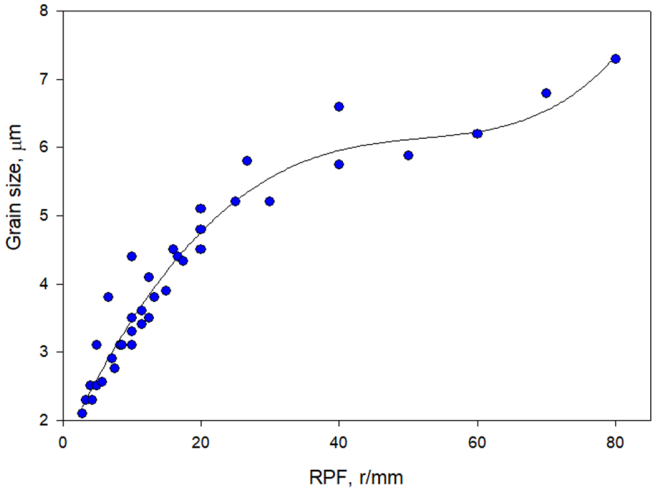

Fig. 7. Variation of grain size of the stir zone with RPF.

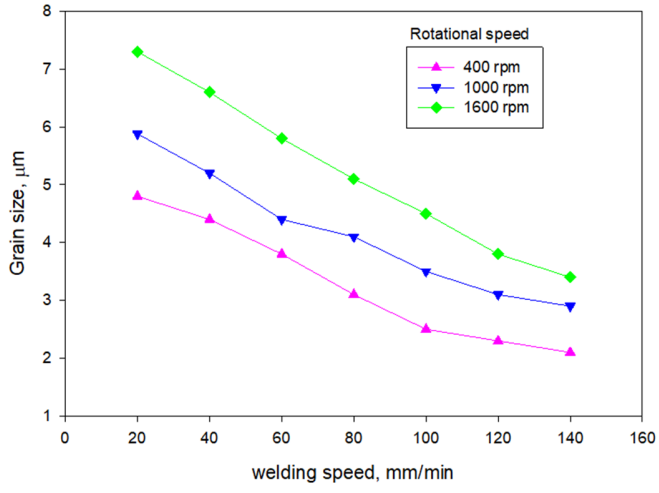

Fig. 8. Variation of grain size of the stir zone with welding speed.

Authors in [12] found that the strength of all stir zones of aluminum joints created by FSW is lower than that of the base material, even when using optimized parameters. Figure 10 illustrates the variation in ultimate tensile strength with respect

to rotational speed across three welding speeds: 20 mm/min, 80 mm/min, and 140 mm/min. At a low welding speed of 20 mm/min, the ultimate strength increases with a rotational speed up to 800 rpm. Beyond that, however, it decreases. At a welding speed of 80 mm/min, the ultimate strength reaches a maximum value of 210 MPa at 1200 rpm and then decreases as the rotational speed increases. At a higher welding speed of 140 mm/min, however, the optimum ultimate tensile strength is 187 MPa at a rotational speed of 1400 rpm. A slight drop in the ultimate tensile strength of the welded joint (182 MPa) occurred as the rotational speed increased to 1600 rpm. Figure 11 portrays the variation in ultimate tensile strength with welding speed at three rotational speeds: 400, 1000, and 1600 rpm. The ultimate tensile strength increases with rotational speed up to an optimal welding speed and then decreases as the welding speed increases. It is observed that the optimal welding speed increases with increasing rotational speed. The maximum ultimate tensile strength (205 MPa) was obtained at a rotational speed of 1000 rpm and a welding speed of 100 mm/min.

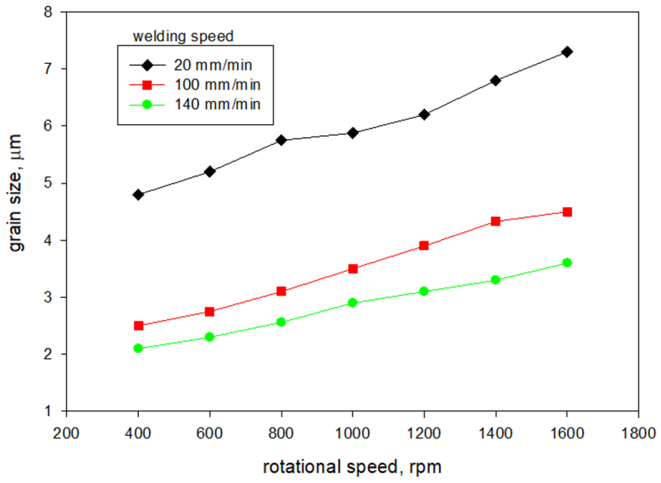

Fig. 9. Variation of grain size of the stir zone with rotational speed.

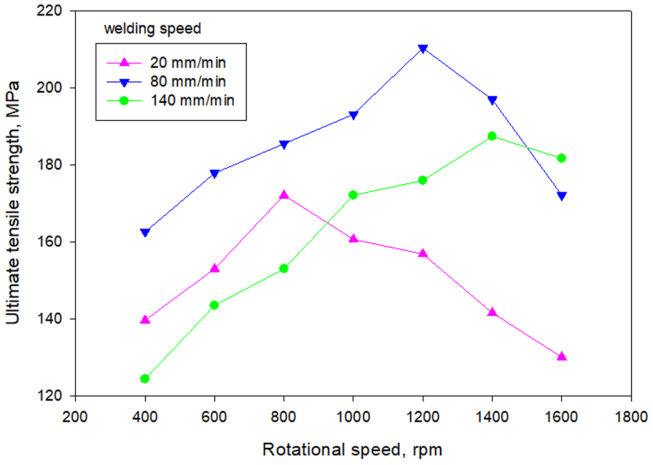

Fig. 10. Variation of ultimate tensile strength with rotational speed.

The heat generated during the welding process and introduced to the welding area affects the tensile strength of the welded joints. Excessive heat reduces the tensile strength of the welded joints [18]. Input heat to the welded area can be increased using two methods: increasing the rotational speed or decreasing the welding speed. As exhibited in Figures 10 and 11, a high welding speed of 140 mm/min requires a high rotational speed of 1400 rpm to reach an optimum ultimate tensile strength of 210 MPa. At a low welding speed of 20 mm/min, a rotational speed of 800 rpm is suitable for achieving an optimum ultimate tensile strength of 172 MPa. This could be attributed to the decrease in heat generated during welding as the rotational speed decreased, leading to the strengthening of materials through the grain boundary strengthening mechanism. However, authors in [32] reported that the strength of the welded joints was approximately 75% that of the base materials at optimized welding parameters.

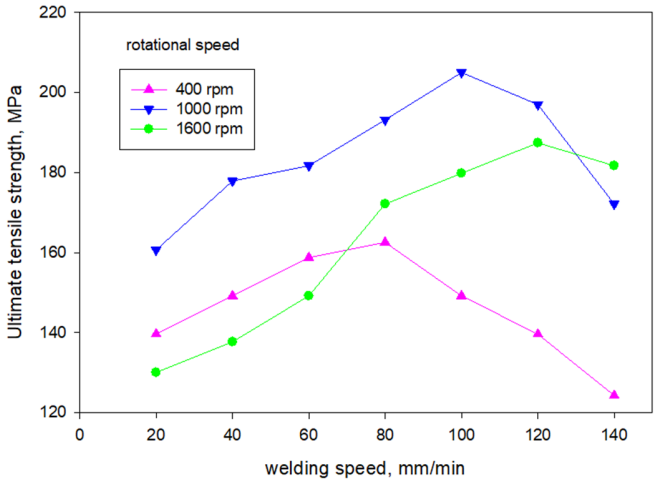

Fig. 11. Variation of ultimate tensile strength with welding speed.

In this study, the optimum yield and ultimate tensile strength of the stir zone were found around 68% of the base material values for the range of welding and rotational speeds used. For metallic materials, grain boundary strengthening, also known as Hall-Petch strengthening, is:

$$\sigma = \sigma_0 + Kd^{-1/2} \quad (1)$$

where σ_0 is the friction stress, K is the coefficient of strengthening, and d is the grain size [33]. Figure 12 presents the correlation between yield strength and the inverse square root of grain size across all welded joints fabricated with various combinations of welding and rotational speeds (42 combinations). The relationship was linear, with a friction stress of 35.45 MPa and a strengthening coefficient of 105.32 MPa·m². Increasing the welding speed while keeping the rotational speed constant decreases the RPF, representing the friction heat introduced per unit weld length [34]. Figure 13 shows how the ultimate tensile strength of the welded joints varies with RPF. The curve can be divided into three zones. In the first zone, where RPF is less than 15 r/mm, the ultimate tensile strength increases with RPF. However, in the second zone, where the RPF values range from 15 to 40 r/mm, the

ultimate tensile strength does not monotonically increase with RPF, due to some RPF values that result from different combinations of rotational and welding speeds. For example, an RPF of 20 r/mm results from a combination of 400 rpm and 20 mm/min. For this value, the tensile strength is 139.6 MPa. Another combination is 1600 rpm and 80 mm/min, where the tensile strength is 172 MPa. In the third zone, where RPF is greater than 40 r/mm, tensile strength decreases as RPF increases. At higher RPF values, such as 40 r/mm, additional frictional heat is introduced into the welding zone during FSW, leading to greater softening of the aluminum in the welding area and a decrease in ultimate tensile strength [35].

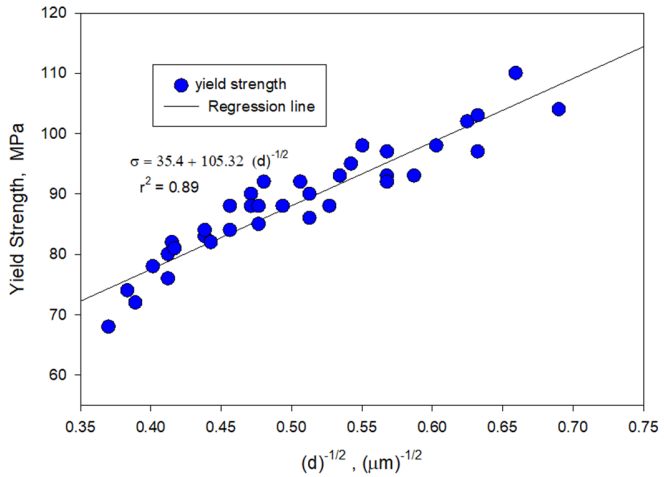

Fig. 12. Hall-Petch strengthening for all the welded joints.

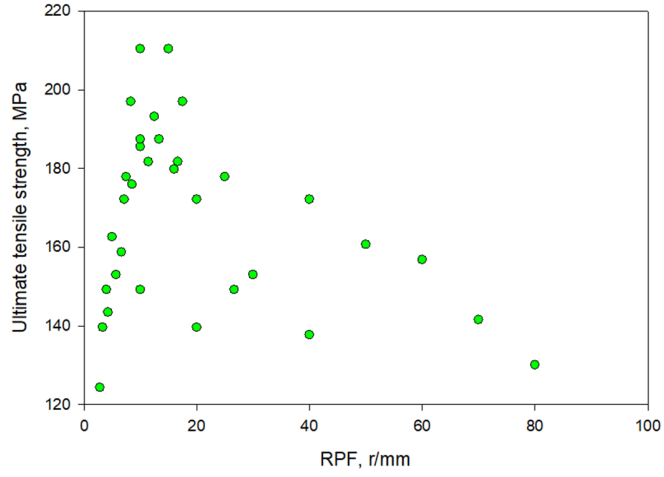

Fig. 13. Variation of ultimate tensile strength with RPF.

The amount of heat dissipated from the piecework during the FSW process depends on the distance traveled by the welding tool per revolution along the welding line. A larger area is exposed to natural air and begins to cool as a result. There are two methods of increasing FPR: keeping the welding speed constant while decreasing the rotational speed or increasing the welding speed while maintaining a constant rotational speed. Authors in [19] revealed that increasing the rotational speed beyond 1300 rpm results in defective welds, while increasing the welding speed beyond 1200 mm/min decreases joint strength. Microhardness is measured and recorded at the stir zone of friction-stir-welded specimens. Figure 14 illustrates the effect of welding speed on the microhardness of the stir zone. The Vickers microhardness of the stir zone increases with increasing welding speed. However, higher welding speeds are associated with lower heat input to the stir zone, resulting in a faster cooling rate in the welded joints. Additionally, readings from the stir zone indicate that microhardness decreases as rotational speed increases at a constant welding speed (Figure 15). This trend was observed in all tested specimens, due to an increase in heat input per unit length associated with an increase in rotational speed.

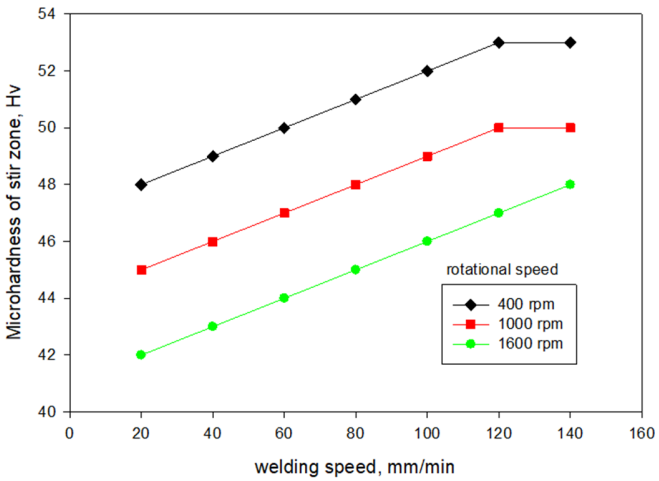

Fig. 14. Variation of microhardness of stir zone with welding speed.

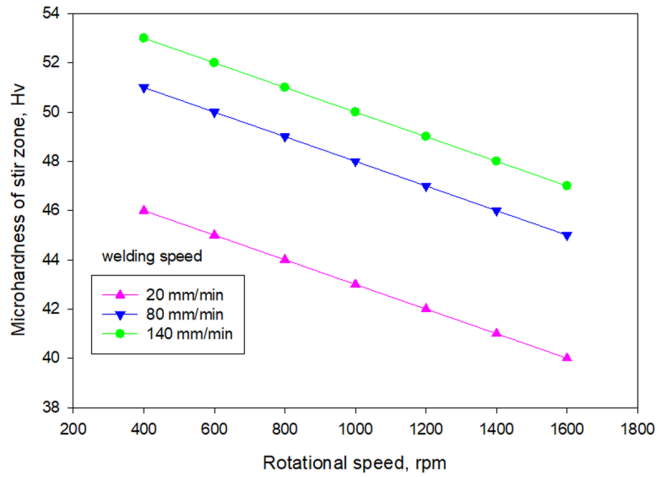

Fig. 15. Variation of microhardness of stir zone with rotational speed.

Stir zone hardness is related to the evolution of the microstructure under the influence of welding parameters. The amount of the heat input to the welding zone significantly affects hardness. Figure 16 shows how the hardness of the stir zone varies with RPF. As evidenced, microhardness decreases as RPF increases.

IV. CONCLUSIONS

The quality of aluminum 5083 alloy friction stir welds depends on the balance between the heat generated and dissipated during welding. This study examines a wide range of welding and rotational speeds to increase the flexibility of correlating generated and dissipated heat.

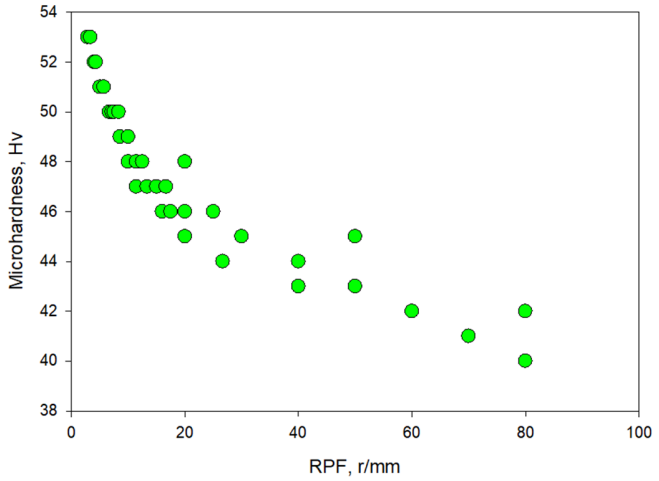

Fig. 16. Variation of microhardness with RPF.

The main conclusions are:

- The amount of heat generated depends on the rotational speed, while the amount of heat dissipated depends on the welding speed. These two parameters can be related to each other using Rotation Per Feed (RPF).
- A sufficient amount of heat can be generated and introduced to the welding area by controlling the RPF, which results in defect-free welded joints.
- The stir zone has a fine microstructure with a grain size of 2.1 µm when RPF is about 2.85 r/mm. At a high RPF value (80 r/mm), the grain size becomes coarser, reaching 7.3 µm.
- The strength of the A5083 alloy base metal is greater than that of the welded joints prepared by Friction Stir Welding (FSW).
- The ultimate tensile strength obtained varies with different combinations of rotational and welding speeds at RPF values between 12 and 18 r/mm.
- The maximum ultimate tensile strength for welded joints (210 MPa) is obtained at a rotational speed of 1200 rpm and a welding speed of 80 mm/min.
- The microhardness of the stir zone for A5083 alloy welded joints decreases with increasing rotational speed due to an increase in heat input per unit length, which leads to coarse grains.

This research covers a wide range of RPF values, from 2.85 r/mm to 80 r/mm, providing an effective approach for selecting optimal combinations of rotational and welding speeds to achieve sound welded joints.

DECLARATION OF COMPETING INTERESTS

The authors declare that they have no competing financial or personal interests that could have influenced the research paper.

ACKNOWLEGDMENT

Not applicable in this work.

DATA AVAILABILITY

The data used in this study are available from the corresponding author upon reasonable request.

REFERENCES

[1] T. Hirata *et al.*, "Influence of friction stir welding parameters on grain size and formability in 5083 aluminum alloy," *Materials Science and Engineering: A*, vol. 456, no. 1, pp. 344–349, May 2007, https://doi.org/10.1016/j.msea.2006.12.079.

[2] A. R. I. Kheder, G. S. Marahleh, and D. M. K. Jamea, "Strengthening of aluminum by SiC, Al2O3 and MgO," *Jordan Journal of Mechanical and Industrial Engineering*, vol. 5, no. 6, pp. 533–541, 2011.

[3] T. Teker, T. Soysal, and G. Akgün, "Effect of rotary friction welding on mechanical properties of 6060 Al alloy," *Revista de Metalurgia*, vol. 57, no. 4, 2021, Art. no. e206, https://doi.org/10.3989/revmetalm.206.

[4] K. Elangovan and V. Balasubramanian, "Influences of tool pin profile and tool shoulder diameter on the formation of friction stir processing zone in AA6061 aluminum alloy," *Materials and Design*, vol. 29, no. 2, pp. 362–373, 2008, https://doi.org/10.1016/j.matdes.2007.01.030.

[5] [5] T. Zhang, Y. He, Q. Shao, H. Zhang, and L. Wu, "Comparative study on fatigue properties of friction stir welding joint and lap joint," in *Proceedings of the 13th International Conference on Fracture*, Beijing, China, 2013.

[6] A. Prince, "Hydrogen solubility in liquid and solid pure aluminum: Critical review of measurement methodologies and reported values," *Materials Sciences and Applications*, vol. 13, no. 4, pp. 158–212, 2022, https://doi.org/10.4236/msa.2022.134010.

[7] A. Squillace, A. De Fenzo, G. Giorleo, and F. Bellucci, "A comparison between FSW and TIG welding techniques: Modifications of microstructure and pitting corrosion resistance in AA 2024-T3 butt joints," *Journal of Materials Processing Technology*, vol. 152, no. 1–3, pp. 97–105, 2004, https://doi.org/10.1016/j.jmatprotec.2004.04.042.

[8] R. S. Mishra and Z. Y. Ma, "Friction stir welding and processing," *Materials Science and Engineering: R: Reports*, vol. 50, no. 1–2, pp. 1–78, 2005, https://doi.org/10.1016/j.mser.2005.07.001.

[9] T. Soysal, "A new solidification cracking test: Stationary weld-pool deformation test," *Science and Technology of Welding and Joining*, vol. 26, no. 7, pp. 622–630, 2021, https://doi.org/10.1080/13621718.2021.1914901.

[10] Y. J. Kwon, I. Shigematsu, and N. Saito, "Dissimilar friction stir welding between magnesium and aluminum alloys," *Materials Letters*, vol. 62, nos. 23–24, pp. 3827–3829, 2008, https://doi.org/10.1016/j.matlet.2008.04.124.

[11] S. A. Khodir and T. Shibayanagi, "Friction stir welding of dissimilar AA2024 and AA7075 aluminum alloys," *Materials Science and Engineering: B*, vol. 148, nos. 1–3, pp. 82–87, 2008, https://doi.org/10.1016/j.mseb.2007.09.024.

[12] L. M. Shehadeh and I. S. Jalham, "The effect of adding different percentages of manganese Mn and copper Cu on the mechanical behavior of aluminum," *Jordan Journal of Mechanical and Industrial Engineering*, vol. 10, no. 1, pp. 19–26, 2016.

[13] K. Harachai and S. Prasomthong, "Investigation of the optimal parameters for butt joints in a friction stir welding process with dissimilar aluminum alloys," *Materials Research Express*, vol. 10, no. 2, 2023, Art. no. 026514, https://doi.org/10.1088/2053-1591/acbb54.

[14] [G. H. Li, L. Zhou, S. F. Luo, Z. Y. Du, J. C. Feng, and F. X. Meng, "Microstructure and mechanical properties of self-reacting friction stir

welded AA2219-T87 aluminium alloy," *Science and Technology of Welding and Joining*, vol. 25, no. 2, pp. 142–149, 2020, https://doi.org/10.1080/13621718.2019.1679681.

[15] Y. K. Yousif, K. M. Daws, and B. I. Kazem, "Prediction of stir welding characteristics using neural network," *Jordan Journal of Mechanical and Industrial Engineering*, vol. 2, no. 3, pp. 151–155, 2008.

[16] J. Luo, J. F. Xiang, L. Yuan, H. X. Lin, X. R. Wu, and D. Z. Xie, "Heat transfer and metal flow behavior of AA7075 high-strength aluminum alloy in a new current-induced friction stir welding with a multi-physics field model based on the inverse method and parameter scanning batch processing technique," *The International Journal of Advanced Manufacturing Technology*, vol. 111, nos. 9–10, pp. 2615–2635, 2020, https://doi.org/10.1007/s00170-020-06249-y.

[17] T. Teker and E. M. Karakurt, "Examination of mechanical properties of high chromium white cast iron/AISI 1030 steel welded by friction welding with nickel interlayer," *Science and Technology of Welding and Joining*, vol. 25, no. 2, pp. 150–156, 2020, https://doi.org/10.1080/13621718.2019.1679682.

[18] M. A. E. Omer, M. Rashad, A. H. Elsheikh, and E. A. Showaib, "A review on friction stir welding of thermoplastic materials: Recent advances and progress," *Welding in the World*, vol. 66, no. 1, pp. 1–25, 2022, https://doi.org/10.1007/s40194-021-01178-0.

[19] J. A. Al-Jarrah, S. Sawalha, T. A. Mansour, M. Ibrahim, M. Al-Rashdan, and D. A. Al-Qahsi, "Welding quality and mechanical properties of aluminum alloys joints prepared by friction stir welding," *Journal of Materials Engineering and Performance*, vol. 23, no. 3, pp. 929–936, 2014, https://doi.org/10.1007/s11665-014-0865-9.

[20] U. Abdul Khaliq *et al.*, "A review on friction stir butt welding of aluminum with magnesium: A new insight on joining mechanisms by interfacial enhancement," *Journal of Materials Research and Technology*, vol. 27, pp. 4595–4624, Nov. 2023, https://doi.org/10.1016/j.jmrt.2023.10.158.

[21] G. G. de Sousa, P. L. C. de Carvalho, I. J. Marques, H. R. Araújo, T. F. de Abreu Santos, and A. de Albuquerque Vicente, "Application of a numeric pure thermal model for prediction of temperature fields in a UNS S32205 duplex steel friction stir welded joint," in *Proceedings of the 75th ABM Annual Congress*, 2022, https://doi.org/10.5151/2594-5327-34689.

[22] K. Elangovan, V. Balasubramanian, and S. Babu, "Predicting tensile strength of friction stir welded AA6061 aluminium alloy joints by a mathematical model," *Materials and Design*, vol. 30, no. 1, pp. 188–193, 2009, https://doi.org/10.1016/j.matdes.2008.04.037.

[23] H. L. Hao *et al.*, "Effect of welding parameters on microstructure and mechanical properties of friction stir welded Al–Mg–Er alloy," *Materials Science and Engineering: A*, vol. 559, pp. 889–896, Jan. 2013, https://doi.org/10.1016/j.msea.2012.09.041.

[24] B. Senthamaraikannan and J. Krishnamoorthy, "Material flow and mechanical properties of friction stir welded AA 5052-H32 and AA6061-T6 alloys with Sc interlayer," *Materials Testing*, vol. 65, no. 7, pp. 1127–1142, 2023, https://doi.org/10.1515/mt-2022-0352.

[25] R. Kosturek, L. Śnieżek, J. Torzewski, and M. Wachowski, "The influence of welding parameters on macrostructure and mechanical properties of Sc-modified AA2519-T62 FSW joints," *Manufacturing Review*, vol. 7, 2020, Art. no. 28, https://doi.org/10.1051/mfreview/2020025.

[26] A. Garg, M. Raturi, and A. Bhattacharya, "Influence of additional heating in friction stir welding of dissimilar aluminum alloys with different tool pin profiles," *The International Journal of Advanced Manufacturing Technology*, vol. 105, nos. 1–4, pp. 155–175, 2019, https://doi.org/10.1007/s00170-019-04186-z.

[27] J. A. Al-jarrah, A. Ibrahim, and S. Sawlaha, "Effect of Applied Pressure on the Mechanical Properties of 6061 Aluminum Alloy Welded Joints Prepared by Friction Stir Welding," *Engineering, Technology & Applied Science Research*, vol. 7, no. 3, pp. 1619–1622, June 2017, https://doi.org/10.48084/etasr.1124.

[28] T. Sun, Y. Shen, R. Ni, W. Hou, Y. Yan, and F. Cao, "Influences of process parameters on morphology and mechanical properties of FSW T-joint of 2024/5083 Al alloy sheets," *Journal of Materials Research and Technology*, vol. 17, pp. 15195–15208, 2022, https://doi.org/10.1016/j.jmrt.2022.02.086.

[29] R. Rudrapati, "Effects of welding process conditions on friction stir welding of polymer composites: A review," *Composites Part C: Open Access*, vol. 8, 2022, Art. no. 100269, https://doi.org/10.1016/j.jcomc.2022.100269.

[30] O. S. Salih, H. Ou, and W. Sun, "Heat generation, plastic deformation and residual stresses in friction stir welding of aluminium alloy," *International Journal of Mechanical Sciences*, vol. 238, 2023, Art. no. 107827, https://doi.org/10.1016/j.ijmecsci.2022.107827.

[31] M. M. Z. Ahmed, M. M. El-Sayed Seleman, D. Fydrych, and G. Çam, "Friction stir welding of aluminum in the aerospace industry: The current progress and state-of-the-art review," *Materials*, vol. 16, no. 8, 2023, Art. no. 2971, https://doi.org/10.3390/ma16082971.

[32] S. Kilic, F. Ozturk, and M. F. Demirdogen, "A comprehensive literature review on friction stir welding: Process parameters, joint integrity, and mechanical properties," *Journal of Engineering Research*, vol. 13, no. 1, pp. 122–130, 2025, https://doi.org/10.1016/j.jer.2023.09.005.

[33] H. Izadi, R. Sandström, and A. P. Gerlich, "Grain growth behavior and Hall–Petch strengthening in friction stir processed Al 5059," *Metallurgical and Materials Transactions A*, vol. 45, no. 12, pp. 5645–5655, 2014, https://doi.org/10.1007/s11661-014-2519-z.

[34] D. Klobčar, L. Kosec, A. Pietras, and A. Smolej, "Friction stir welding of aluminium alloy 5083," *Materials and Technology*, vol. 46, no. 1, pp. 25–30, 2012.

[35] V. Balasubramanian, "Relationship between base metal properties and friction stir welding process parameters," *Materials Science and Engineering: A*, vol. 480, nos. 1–2, pp. 397–403, 2008, https://doi.org/10.1016/j.msea.2007.07.039.